J. Fluid Mech. (2015), *vol.* 778, R4, doi:10.1017/jfm.2015.400

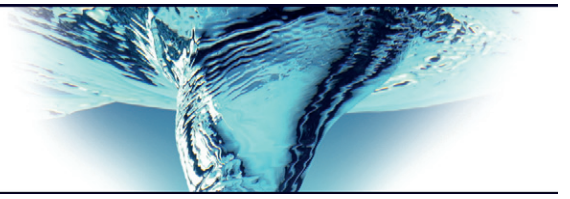

JFM RAPIDS
journals.cambridge.org/rapids

Dynamics of the large-scale circulation in turbulent Rayleigh–Bénard convection with modulated rotation

Jin-Qiang Zhong[1,†], **Sebastian Sterl**[1,2] **and Hui-Min Li**[1]

[1]Shanghai Key Laboratory of Special Artificial Microstructure Materials and Technology and School of Physics Science and Engineering, Tongji University, Shanghai 200092, China

[2]Physics of Fluids Group, Faculty of Science and Technology, University of Twente, PO Box 217, 7500 AE Enschede, The Netherlands

(Received 29 April 2015; revised 29 June 2015; accepted 9 July 2015;
first published online 4 August 2015)

We present measurements of the azimuthal rotation velocity $\dot{\theta}(t)$ and thermal amplitude $\delta(t)$ of the large-scale circulation in turbulent Rayleigh–Bénard convection with modulated rotation. Both $\dot{\theta}(t)$ and $\delta(t)$ exhibit clear oscillations at the modulation frequency ω. Fluid acceleration driven by oscillating Coriolis force causes an increasing phase lag in $\dot{\theta}(t)$ when ω increases. The applied modulation produces oscillatory boundary layers and the resulting time-varying viscous drag modifies $\delta(t)$ periodically. Oscillation of $\dot{\theta}(t)$ with maximum amplitude occurs at a finite modulation frequency ω^*. Such a resonance-like phenomenon is interpreted as a result of optimal coupling of $\delta(t)$ to the modulated rotation velocity. We show that an extended large-scale circulation model with a relaxation time for $\delta(t)$ in response to the modulated rotation provides predictions in close agreement with the experimental results.

Key words: Bénard convection, rotating flows, turbulent convection

1. Introduction

Turbulent convection occurs in a variety of astrophysical and geophysical flows, including convection in the ocean (Marshall & Schott 1999), in the outer layer of the Sun (Miesch 2000), and in the fluid cores of the Earth and other terrestrial planets (Busse 2000; Olson 2013). Many planetary bodies in the solar system undergo time-dependent rotations. For instance, the spinning rate of Mercury exhibits oscillations dominated by an 88-day periodicity. It is expected that the resulting librating force strongly influences the convective dynamo process in its fluid core that sustains Mercury's global magnetic field (Koning & Dumberry 2013). Furthermore, variation of the Earth's rotation speed occurs due to the change of polar ice sheets

†Email address for correspondence: jinqiang@tongji.edu.cn

between ice and non-ice ages (Doake 1977), which may produce perturbations to the outer-core convection and lead to the observed temporal variations of the geomagnetic field (Miyagoshi & Hamano 2013).

Turbulent Rayleigh–Bénard convection (RBC) in a fluid heated from below has been studied extensively as a paradigmatic model for turbulent convection in recent years (Ahlers, Grossmann & Lohse 2009; Lohse & Xia 2010; Chillá & Schumacher 2012). The main component of the fluid flow in turbulent RBC is a large-scale circulation (LSC) in a vertically oriented plane that consists of buoyant plumes detached from the thermal boundary layers (see e.g. Krishnamurti & Howard 1981; Niemela, Babuin & Sreenivasan 2001; Sreenivasan, Bershadskii & Niemela 2002; Funfschilling & Ahlers 2004; Brown, Nikolaenko & Ahlers 2005; Xi *et al.* 2009). An important feature of the LSC is the dynamical change of the azimuthal orientation of its circulation plane, which includes erratic reorientations, such as cessations and reversals (Sreenivasan *et al.* 2002; Araujo, Grossmann & Lohse 2005; Brown *et al.* 2005), originated from stochastic turbulent fluctuations in the background flow, as well as azimuthal motions governed by deterministic fluid momentum transport equations (Hart, Kittelman & Ohlsen 2002; Brown & Ahlers 2006, 2007, 2008; Kunnen, Clercx & Geurts 2008).

To our knowledge, to date, the azimuthal motion of the LSC has been investigated experimentally only in the context of time-independent forcing. Examples include the Coriolis force in constant-rotation convection (Hart *et al.* 2002; Brown & Ahlers 2006; Kunnen *et al.* 2008; Zhong & Ahlers 2010), and the fluid pressure gradients due to the azimuthal asymmetry of the flow field created in samples with non-circular cross-sections (Song *et al.* 2014). Under these conditions the fluid acceleration is quickly damped in the presence of the viscous dissipation from the boundary layers (BLs) and does not significantly impact the LSC flow. How the LSC dynamics is influenced by azimuthal fluid acceleration therefore still remains an open question.

Several fluid models have been developed to describe the dynamics of the LSC, including stochastic models that interpret flow reversal as a random diffusion process of the LSC strength in a potential well (Sreenivasan *et al.* 2002), and deterministic models based on fluid momentum equations that predict oscillations of the LSC direction (Resagk *et al.* 2006) and cessations (Araujo *et al.* 2005). In order to describe the rich azimuthal dynamics of the LSC, a model consisting of two stochastic differential equations, respectively, the LSC azimuthal velocity $\dot{\theta}$ and thermal amplitude δ, was developed (Brown & Ahlers 2007, 2008). The model has provided predictions for aspects of the LSC dynamics such as diffusive meandering and erratic reorientation observed in experiments (Brown *et al.* 2005; Song *et al.* 2014). Recently, this model was extended to include rotation effects and calculate the cessation frequency and the probability distribution of δ in rotating RBC (Assaf, Angheluta & Goldenfeld 2012). These theoretical results were in close agreement with the experimental observations (Zhong & Ahlers 2010).

Earlier experiments have been devoted to study the influence of modulated rotation on the convection instability in RBC. Niemela, Smith & Donnelly (1991) reported that suppression of the convective instability took place only in a certain frequency range in which the modulation period is close to the momentum diffusion time across the viscous BL. Outside of this range, modulated rotation was found to result in an apparent destabilization effect, lowering the threshold for onset of convection. Thompson, Bajaj & Ahlers (2002) studied the effect of modulated rotation rates on the onset of the Kuppers–Lortz (KL) instability. It was found that the modulation of the rotation could prevent the KL instability from occurring, replacing the chaotic patterns by concentric ring-shaped patterns that are generated at the cylinder boundary.

Furthermore, an experimental investigation of the heat transport in turbulent RBC in the presence of modulated rotation was performed by Niemela, Babuin & Sreenivasan (2010). A sharp transition to a state of enhanced heat transport was observed at significantly large modulation amplitudes. Recent numerical simulations (Geurts & Kunnen 2014) elucidated how the enhanced heat transport in turbulent RBC is due to reorganizations of the thermal flow structures under rapidly modulated rotations. The influence of modulated rotation on the flow fields has also been investigated both experimentally and theoretically in the context of Taylor–Couette systems (see e.g. Donnelly 1964; Hall 1975; Avila *et al.* 2008).

In this paper we present investigations of the LSC dynamics in turbulent RBC when the fluid is subjected to librating rotations. We focus on the dynamical response of the LSC azimuthal velocity $\dot{\theta}$ when fluid acceleration is created by oscillating Coriolis force, and the time-dependent LSC thermal amplitude δ driven by oscillatory viscous BLs. We proceed as follows. In § 2 we describe the experimental apparatus and methods. Section 3.1 presents results pertaining to oscillations of the LSC azimuthal orientation $\theta(t)$ and velocity $\dot{\theta}(t)$. Experimental results are compared with theoretical predictions from a one-dimensional model. In § 3.2 we discuss oscillations of the LSC thermal amplitude δ. We extended the LSC model (Brown & Ahlers 2007, 2008), considering a rotation-dependent thickness of the viscous BLs and a finite relaxation time τ for $\delta(t)$ in response to the oscillating BL thickness. The model predictions are in good agreement with the experimental results. In § 3.3 we report the resonant response in $\dot{\theta}(t)$ observed in an intermediate modulation frequency regime, which can also be interpreted qualitatively with our model. A brief summary and discussion of the results is provided in § 4.

2. Experimental apparatus and methods

The experiment was performed with a constant Rayleigh number $Ra \equiv \alpha g \Delta T L^3/\kappa\nu = 8.24 \times 10^9$ (g is the gravitational acceleration, α, ν and κ are the thermal expansion coefficient, the viscosity and thermal diffusivity of water, ΔT is the applied temperature difference and L is the sample height) and a constant Prandtl number $Pr \equiv \nu/\kappa = 4.38$. We used a convection sample that had a similar design to the apparatus described in Zhong *et al.* (2009) and Zhong & Ahlers (2010). It had circular top and bottom plates made of oxygen-free copper (OFHC, TU1). The sample was filled with deionized water at a mean temperature of 40.00 °C. It had a diameter $D = 24.1$ cm and a height $L = 24.0$ cm, yielding an aspect ratio of 1.00. The Plexiglas (Lexan) sidewall, 0.4 cm in thickness, was fitted into a groove in each copper plate. Three rows of eight thermistors, equally spaced azimuthally and lined up in vertical columns at heights $L/4$, $L/2$ and $3L/4$, were placed into the sidewall so as to be within $d = 0.08 \pm 0.01$ cm from the fluid surface. We measured the temperature of each thermistor T_i with a sampling frequency of 4.0 s, and fitted the function $T_i = T_0 + \delta \cos(\mathrm{i}\pi/4 - \theta)$, $i = 1, \ldots, 8$, to the eight temperatures in each row. Following this experimental protocol, we determined the LSC thermal amplitude $\delta(t)$ and the azimuthal orientation $\theta(t)$ of its circulating plane (Brown *et al.* 2005). The results shown here are from the middle-row thermistors unless stated otherwise.

The convection sample was mounted on a rotary table. When working in a modulation mode, the rotating velocity of the sample varied according to $\Omega = \Omega_0[1 + \beta \cos(\omega t)]$. We chose $\Omega_0 = 0.104$ rad s^{-1} and $\beta = 0.212$, so the Rossby number $Ro = \sqrt{(\alpha g \Delta T/L)}/2\Omega$ varied periodically in the range $(0.31 \leqslant 1/Ro \leqslant 0.51)$ in the presence of modulation. As depicted in grey in figure 1(*a*), in this range the

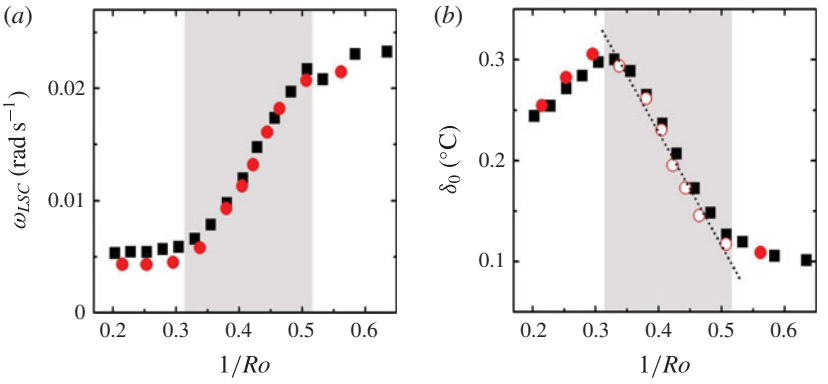

FIGURE 1. Dynamical properties of the LSC when the sample rotates at constant rate. (*a*) The mean retrograde rotation velocity ω_{LSC} as a function of $1/Ro$. (*b*) The mean LSC amplitude δ as a function of $1/Ro$. Symbols: black squares, experimental data from Zhong & Ahlers (2010) with $Ra = 8.97 \times 10^9$; red circles, the present work with $Ra = 8.24 \times 10^9$. The range in which we perform the modulated rotation experiment is indicated in grey. The dashed line in (*b*) is a linear fit to the open circles, through which we determine $\chi(1/Ro) = \delta(1/Ro)/\delta(0) = -5.1/Ro + 3.1$ in (3.2) and (3.3).

LSC retrograde rotation rate ω_{LSC} and the thermal amplitude δ exhibit the maximum responses to variations in Ω. The normalized modulation rate ω/Ω_0 ranged from 0.025 to 1.0. The LSC flow velocity in its circulating plane, $U \approx 1.5$ cm s^{-1}, was determined by the LSC turnover time measured through the autocorrelation functions of the sidewall temperatures (Zhong & Ahlers 2010). Thus the Strouhal number $Sr = L\dot{\Omega}/4\Omega U$, which measures the ratio of the Euler force and the Coriolis force, did not exceed 0.08.

Thermistors embedded within the top and bottom conductive plates were calibrated simultaneously in a separate apparatus against a laboratory standard platinum thermometer traceable to the ITS-90 temperature scale, with a precision better than 0.002 °C. In each of the conductive plates, there was one thermistor at the plate centre, and six thermistors equally spaced on a circle of 21.0 cm in diameter. The temperature inhomogeneity on each conductive plate, as measured by these thermistors, was within one or two per cent of ΔT during the experiment. Calibration of the 24 sidewall thermistors was conducted against the top- and bottom-plate thermistors.

The finite thermal diffusion process through the sidewall to the thermistors in it causes a time delay in our measurements of the fluid temperature. The main time delay between the instantaneous fluid temperature and the temperature measured by the sidewall thermistors is estimated to be $d^2/\kappa_s \approx 4.6$ s (κ_s is the sidewall thermal diffusivity). Such a time delay has been taken into account in determining $\phi_{\dot{\theta}}$ and ϕ_δ discussed in figures 4 and 5(*a*). Such corrections are much less than the standard deviation of $\phi_{\dot{\theta}}$ and ϕ_δ.

3. Results

3.1. *Oscillations of the LSC azimuthal orientation θ and velocity $\dot{\theta}$*

Figure 2(*a*) shows a time series of θ for $\omega/\Omega_0 = 0.1$. The azimuthal orientation of the LSC undergoes linear net rotation in the retrograde direction at an average rate ω_{LSC}.

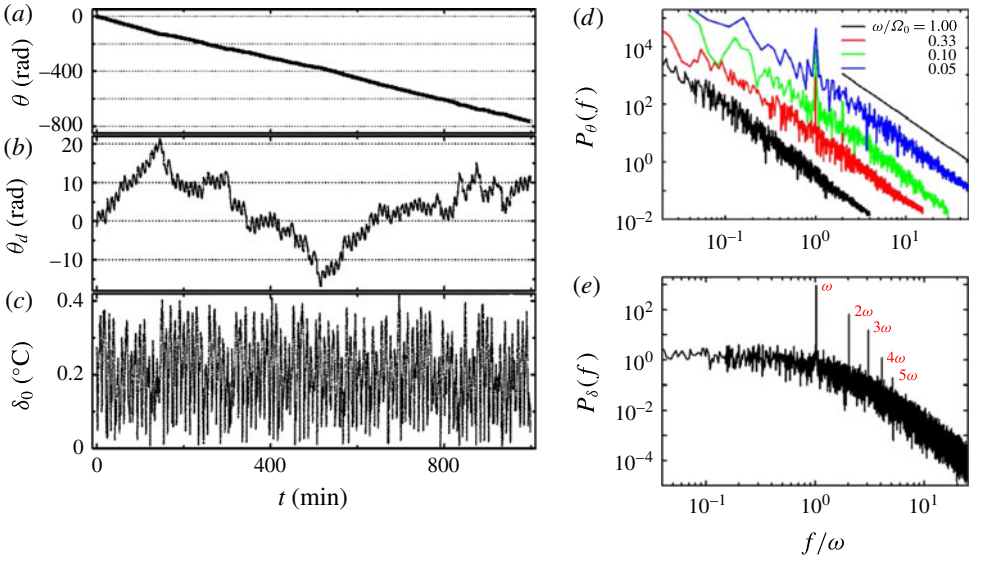

FIGURE 2. Experimental data for $\omega = 0.1\Omega_0$. Time traces (*a*) for $\theta(t)$, (*b*) for the corresponding $\theta_d(t)$ and (*c*) for the thermal amplitude $\delta(t)$. Scaled power spectra (*d*) of $\theta(t)$ and (*e*) of $\delta(t)$. The solid line in (*d*) denotes $P_\theta \sim f^{-2}$.

Within our experimental resolution, ω_{LSC} is determined by Ω_0, but independent of the modulation frequency ω. However, the detrended time series $\theta_d(t) = -\theta(t) - \omega_{LSC}t$ exhibited not only diffusive behaviour in long time scales, but also clear oscillations at the modulation frequency ω (figure 2*b*). Typical power spectra of $\theta_d(t)$, given in figure 2(*d*), show a main peak at $f = \omega$ in a background spectrum falling off as f^{-2}, the latter corresponding to a diffusive meandering of the LSC in the azimuthal direction. The signal-to-noise ratio of the peak for oscillations decreases with increasing ω up to $\omega_c \approx \Omega_0$, beyond which the modulation period $T = 2\pi/\omega$ is less than the turnover time of the LSC. For higher modulation frequencies $\omega \geqslant \omega_c$ the peak at $f = \omega$ in the power spectra disappears and we see no regular oscillation in the time series $\theta_d(t)$.

Similarly, the thermal amplitude δ was also found to consist of oscillations in a random-fluctuation background. An example is plotted in figure 2(*c*) for $\omega/\Omega_0 = 0.1$, with its power spectrum given in figure 2(*e*), wherein higher harmonics appear at $f = (2\omega, \ldots, 5\omega)$ in addition to the main peak at the frequency of modulation.

The principal information of the oscillation phases and amplitudes of $\theta_d(t)$ and $\delta(t)$ resides in their time series dominated by the randomly fluctuating background (figure 2*b*,*c*). In order to discern their general responses to $\Omega(t)$ more clearly, we divide the time series of θ_d and δ according to the modulation periods. Mean values of $\langle\theta_d\rangle$ and $\delta_0 = \langle\delta\rangle$ are subtracted from θ_d and δ. The data are then overlaid in one modulation cycle to compose data 'ensembles'. Modulation periods affected by erratic reorientation events defined as $\delta(t) \leqslant 0.1\delta_0$ (Brown *et al.* 2005) are removed from the regular oscillation data in our analysis. An example of ensembles for $\omega/\Omega_0 = 0.1$ (figure 3*a*,*b*) shows that data points for $\theta_d(t)$ and $\delta(t)$ are mostly collapsed into a sinusoidal curve. Then $\theta_d(t)$ is approximated to an analytical function through a fourth-order Savitzky–Golay method with window length of one modulation cycle.

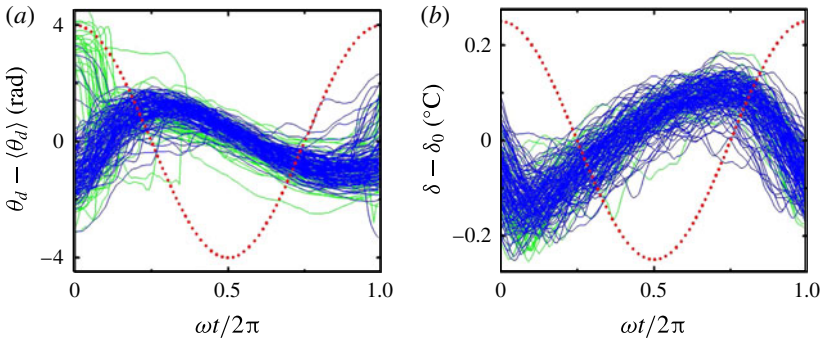

FIGURE 3. Data ensemble (*a*) of $\theta_d(t)$ and (*b*) of $\delta(t)$ for $\omega = 0.1\Omega_0$. Green lines: modulation periods affected by reorientation events, which are removed from the regular oscillation data (blue curves) for analysis. The red dotted curves show $\Omega(t)$ with arbitrary units.

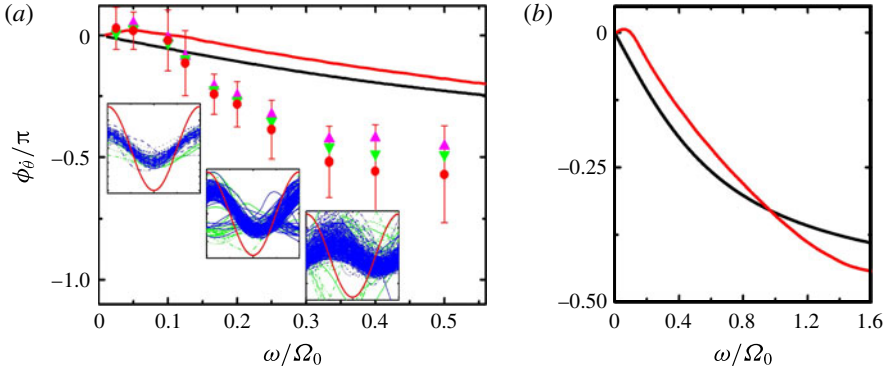

FIGURE 4. (*a*) The phase lag $\phi_{\dot\theta}$ as a function of ω/Ω_0. Experimental data are shown as red circles (from middle-row thermistors), purple triangles (top-row) and green inverted triangles (bottom-row). Error bars denote the standard deviation. Black curve: the asymptotic solution of (3.1), $\phi_{\dot\theta} = -\tan^{-1}(\omega/(3\nu Re/4L^2 + 9\nu Re^{1/2}/L^2))$. Red curve: numerical solutions for (3.2) and (3.3). Insets: data ensembles for $\dot\theta(t) - \dot\theta_0$ displayed in the vertical scale $[-0.04, 0.04]$ (rad s^{-1}). From left to right: $\omega/\Omega_0 = 0.05$, 0.1 and 0.33. (*b*) Extended plot for the theoretical predictions of $\phi_{\dot\theta}$ for $0 \leqslant \omega/\Omega_0 \leqslant 1.6$.

The azimuthal rotation velocity $\dot\theta(t)$ is then extracted from $\theta_d(t)$ through its time derivative.

Figure 4(*a*) contains data ensembles of $\dot\theta$ for three ω values. Despite the variance of $\dot\theta$ about its mean oscillations, one sees that the oscillation phase is sensitive to the modulation frequency: when ω increases, $\dot\theta$ lags behind $\Omega(t)$ increasingly. For a quantitative analysis of its oscillatory response, we fitted $\dot\theta$ in each modulation cycle to $\dot\theta(t) = \dot\theta_0 + A_{\dot\theta}\cos(\omega t + \phi_{\dot\theta})$. Figure 4(*a*) shows $\phi_{\dot\theta}$ as a function of ω/Ω_0. It appears that $\phi_{\dot\theta}$ decreases most rapidly in the regime of $(0.1 \leqslant \omega/\Omega_0 \leqslant 0.3)$ and asymptotically reaches $-\pi/2$ at large ω.

The increasing phase lag in $\dot\theta$ at large ω implies that fluid acceleration plays a role in determining the LSC dynamics. To explain this, an equation of motion for $\dot\theta$ is obtained from the Navier–Stokes equation, in which the LSC azimuthal acceleration is

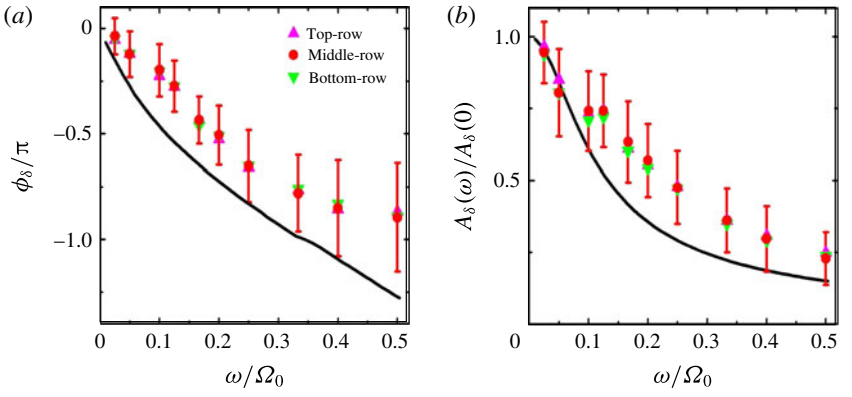

FIGURE 5. (*a*) The phase lag ϕ_δ as a function of ω/Ω_0 measured in the experiments and as obtained from the model (black curve). (*b*) Same as panel (*a*), but for the normalized amplitude $A_\delta(\omega)/A_\delta(0)$. Here $A_\delta(0) = |\delta(\Omega_{max}) - \delta(\Omega_{min})|/2$ is the adiabatic response given in figure 1. Error bars: the standard deviations.

attributed to its rotational inertia, the viscous dissipation and the Coriolis force (Brown & Ahlers 2006):

$$\ddot{\theta} + \left(\frac{3\nu Re}{4L^2} + \frac{9\nu\sqrt{Re}}{L^2}\right)\dot{\theta} - \frac{3\nu Re}{4L^2}\Omega(t) = 0, \tag{3.1}$$

with the Reynolds number $Re = UL/\nu$. When a constant rotation is applied, the azimuthal acceleration $\ddot{\theta}$ is quickly damped by viscous dissipation. Also $\dot{\theta}(t)$ approaches a steady solution proportional to Ω so $\phi_{\dot{\theta}} = 0$. However, when Ω is oscillating at a frequency ω, the acceleration term $\ddot{\theta}$ becomes significant to modify the response of $\dot{\theta}$ at large ω. It is this inertia effect that causes the phase lag in $\dot{\theta}$. The solution of $\phi_{\dot{\theta}}$ for (3.1) is depicted in figure 4(*a*,*b*), which interprets reasonably the observed increasing phase lag when ω increases.

3.2. *Oscillations of the LSC thermal amplitude* δ

Another important aspect of the LSC dynamics in the presence of rotational modulation is the oscillations of its thermal amplitude δ, which is readily seen in its ensemble (figure 3*b*). In order to capture its harmonic features, we fitted $\delta(t)$ within each modulation cycle by $\delta(t) = \delta_0 + A_\delta \cos(\omega t + \pi + \phi_\delta)$, neglecting its high-frequency oscillating components indicated in the power spectrum (figure 2*e*). The term π is included because $\delta(t)$ is anticorrelated to $\Omega(t)$ in the low-frequency limit $\omega \approx 0$ (figure 1*b*). Figure 5 shows ϕ_δ and the normalized amplitude $A_\delta(\omega)/A_\delta(0)$ as functions of ω/Ω_0. We observe that, with increasing ω, $\delta(t)$ lags behind $\Omega(t)$ strongly and A_δ appears to decrease monotonically.

To provide a quantitative interpretation of this oscillatory state, we consider a physical model in which the main degrees of freedom (δ and $\dot{\theta}$) of the LSC flow are governed by two coupled stochastic equations. The formulation of the model follows the prior works in Brown & Ahlers (2007) and Assaf *et al.* (2012), with extensions to include the effects of modulated rotations noted below.

The equation of motion for δ is a Langevin equation,

$$\dot{\delta} = \frac{\delta}{\tau_\delta} - \frac{\delta^{3/2}}{\tau_\delta \delta_0^{1/2} \sqrt{\chi(\Omega')}} + f_\delta(t), \tag{3.2}$$

with $\tau_\delta = L^2/(18\nu Re^{1/2})$, $\delta_0 = 18\pi\Delta T Pr Re^{3/2}/Ra$ and $\chi(\Omega')$ is as specified below. The increment of the LSC flow strength, and hence $\dot{\delta}$, is given by the buoyancy force and the viscous dissipation from the BLs. Similar to the theory mentioned in (3.1), the Langevin equation for $\dot{\theta}$ is coupled to the LSC flow strength U. Assuming U is instantaneously proportional to δ, we obtain

$$\ddot{\theta} = -\left(\frac{\delta}{\tau_{\dot{\theta}}\delta_0} + \frac{\delta^{1/2}}{2\tau_\delta \delta_0^{1/2}\sqrt{\chi(\Omega')}}\right)\dot{\theta} + \frac{\delta}{\tau_{\dot{\theta}}\delta_0}\Omega(t) + f_{\dot{\theta}}(t), \tag{3.3}$$

where $\tau_{\dot{\theta}} = L^2/(2\nu Re)$. The stochastic driving terms f_δ and $f_{\dot{\theta}}$ in both (3.2) and (3.3) model the small-scale turbulent fluctuations. They are assumed to be Gaussian white noise with a mean diffusivity $D_\delta = 3.0 \times 10^{-5}$ (K^2 s^{-2}) and $D_{\dot{\theta}} = 1.0 \times 10^{-5}$ (rad^3 s^{-2}), determined from the experimental data.

We note that the viscous damping for the equations of both δ and $\dot{\theta}$ is caused by dissipation from the viscous BLs. In performing volume averaging, one finds that the magnitudes of these dissipation terms are proportional to $\lambda^{-1}(\Omega)$, with the viscous BL thickness λ dependent on Ω. Over the range of $1/Ro$ studied here ($0.31 \leqslant 1/Ro \leqslant 0.51$), variations of the Ekman layer thickness play a role in influencing the LSC flow. According to linear BL theory, its thickness decreases with increasing Ω, as demonstrated in recent DNS results (Kunnen *et al.* 2011).

We estimate the formation time of the Ekman layer, $\tau_E = \delta_E^2/\nu \approx 9$ s (with $\delta_E = (\nu/\Omega_0)^{1/2}$ is the Ekman layer thickness). It is much shorter than a modulation period. Therefore we can assume that when rotational modulation is applied, variation in λ follows adiabatically its dependence on $\Omega(t)$. Here we introduce a dimensionless variable $\chi(\Omega) = [\lambda(\Omega)/\lambda(0)]^2$ (Assaf *et al.* 2012). It is given by the stationary solution of (3.2) with $\dot{\delta} = 0$ and $\chi(\Omega) = \delta(\Omega)/\delta(0)$. In practice, it is determined from fitting the experimental data of $\delta(1/Ro)$ in the studied regime (figure 1*b*): $\chi(1/Ro) = \delta(1/Ro)/\delta(0) = -5.1/Ro + 3.1$. A scale factor for the BL thickness, $\chi(\Omega)^{-1/2}$, is thus multiplied in the dissipation terms in (3.2) and (3.3). Furthermore, since the LSC flow spans the size of the sample L, the response of its amplitude δ to the variation of the viscous drag from the BLs requires a relaxation time τ. The magnitude of τ is assumed to be of the order of the LSC turnover time $\tau \approx \pi L/U = 50$ s. This time-delay effect is included in the equations, $\Omega'(t) = \Omega(t-\tau)$, in determining the dissipation terms. We close the dynamical system with (3.2) and (3.3), with one unknown parameter $\chi(\Omega)$ determined by direct fitting of the experimental data $\delta(\Omega)$ in figure 1(*b*). We presume that the features of high-order harmonic oscillations shown in the power spectra of both $\delta(t)$ and $\theta(t)$ (figure 2*d*,*e*) are due to the nonlinearity of (3.2) and (3.3).

We compare the model predictions to the experimental results. Figure 4(*a*) shows that, in the experimental range ($0 \leqslant \omega/\Omega_0 \leqslant 0.5$), $\phi_{\dot{\theta}}$ is underestimated by the model. Further investigations of the interplay between modulated rotations and the LSC dynamics in short time scales (such as sloshing and torsional oscillations (Funfschilling & Ahlers 2004; Xi *et al.* 2009)) may provide insight to understand the predominant inertia effect observed. However, the model does predict the increasing phase lag, which approaches $-\pi/2$ in the high-frequency limit, as shown

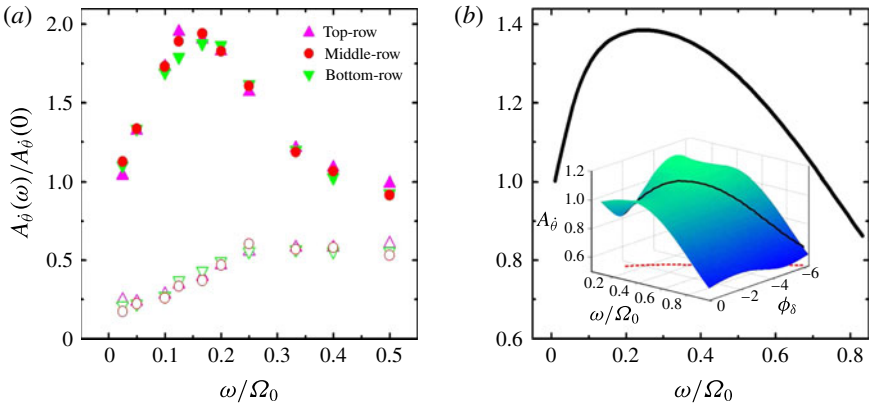

FIGURE 6. Experimental (a) and numerical (b) data for the normalized amplitude $A_{\dot\theta}(\omega)/A_{\dot\theta}(0)$ as a function of ω/Ω_0. Here $A_{\dot\theta}(0) = [\omega_{LSC}(\Omega_{max}) - \omega_{LSC}(\Omega_{min})]/2$ is the adiabatic response given in figure 1. The open symbols in (a) denote the standard deviations of $A_{\dot\theta}$. Inset in (b): amplitude $A_{\dot\theta}(\omega, \phi_\delta)$ as a function of ω/Ω_0 and ϕ_δ. Its solution $A_{\dot\theta}(\omega)$ with the constraint of $\phi_\delta(\omega)$ (dashed red line in the ω–ϕ_δ plane) given in (3.3) is shown as a black curve.

in figure 4(b). We also note that the results from the full dynamical model are in general agreement with the theory in (3.1). They imply that the phase lag in $\dot\theta$ is mainly attributable to the azimuthal fluid acceleration of the LSC flow, but nearly independent of the oscillations of δ. Figure 5 compares the modelling results to the experimental data for ϕ_δ and $A_\delta(\omega)/A_\delta(0)$ in the experimental range of ω/Ω_0. The model predictions are in good accord with the measurements. The phase lag in δ could be explained as mainly due to the finite relaxation time it takes for the bulk circulation to respond to the time-varying BL thickness.

3.3. *Dynamical resonant response in* $\dot\theta$

Finally we point out an interesting finding of the oscillation amplitude of $\dot\theta$ from the experiment that can be reasonably predicted within the framework of our modelling analysis. In figure 6(a) we present experimental data for $A_{\dot\theta}(\omega)/A_{\dot\theta}(0)$ as a function of ω. It is apparent that the dependence of $A_{\dot\theta}$ on ω is non-monotonic. A maximum occurs at $\omega^* = 0.167\Omega_0$ where $A_{\dot\theta}$ is enhanced by as much as 100 %. The appearance of this resonant-like behaviour in $A_{\dot\theta}$ can be understood as a result of optimal coupling of δ and Ω. In the limit of very slow modulations ($\omega \approx 0$) we have $\phi_\delta \approx 0$; and $\dot\theta(t)$ instantaneously follows the time variation in $\Omega(t)$, such that $\dot\theta(t) = \omega_{LSC}(\Omega(t))$ is given by figure 1(a). Thus $A_{\dot\theta}$ approaches the value $A_{\dot\theta}(0)$. Moreover, we derive from (3.3) that in this regime the variation of $A_{\dot\theta}$ due to a small change in ϕ_δ is given by (in the leading order of ϕ_δ): $A_{\dot\theta}(\omega) - A_{\dot\theta}(0) \sim -\sin\phi_\delta$. On the other hand, when $\omega \gg \Omega_0$, A_δ decreases to zero (figure 5b) and correspondingly $A_{\dot\theta} \approx 0$ as well. Therefore we infer that a maximum in $A_{\dot\theta}$ occurs in between these two extremes.

To elucidate more clearly the mutual influences of A_δ and ϕ_δ on $A_{\dot\theta}$, we solved for $A_{\dot\theta}(\omega, \phi_\delta)$ numerically from (3.3) for an oscillating function $\delta(t)$ with arbitrary phases ($0 < \phi_\delta < 2\pi$) and with its amplitude fixed to the solution $A_\delta(\omega)$ given by (3.2). The results of $A_{\dot\theta}(\omega, \phi_\delta)$ are depicted in the inset of figure 6(b), where the non-monotonic dependence of $A_{\dot\theta}$ on ϕ_δ is clarified. The solution $A_{\dot\theta}(\omega)$ to the full dynamical system

(3.2) and (3.3) is then determined with the constraint of $\phi_\delta(\omega)$ given by (3.2). It is depicted in figure 6(*b*) and in its inset as well. Despite the different values of ω^* and the maximum in $A_{\dot\theta}$, the model offers a reasonable prediction of the resonant response of $\dot\theta$. We conclude that oscillation of $\dot\theta$ with a maximum amplitude can be produced in an intermediate ω regime in which $\delta(t)$ has the optimal phase shift from $\Omega(t)$.

4. Discussion

In this paper we present an experimental study of the LSC dynamics in turbulent RBC with modulated rotation. We observe clear oscillations in the LSC azimuthal rotation velocity $\dot\theta(t)$ and thermal amplitude $\delta(t)$. The fluid acceleration driven by oscillating Coriolis force is found, for the first time, to influence the LSC azimuthal motions and cause an increasing phase lag in $\dot\theta(t)$ with respect to $\Omega(t)$ when the modulation frequency increases. It is considered as a manifestation of the inertia effect of the LSC flow in the presence of rotational modulation. Moreover, the applied modulation gives rise to oscillatory BLs and we show that the resulting time-varying viscous drag may modify $\delta(t)$ periodically.

Remarkably, oscillation of the azimuthal rotation velocity $\dot\theta(t)$ with maximum amplitude occurs at modulation frequency $\omega^* = 0.167\Omega_0$. Such a resonance-like phenomenon in a turbulent background is intriguing, since one would expect that, instead of a periodic flow with a single dominant time scale, turbulent flows with a broad frequency spectrum in the fluid interior are driven by the modulated rotations. Presently, a theoretical understanding of the resonant turbulence and the value of ω^* is lacking. However, the proposed linear response theory ((3.2) and (3.3)) provides a reasonable interpretation that the resonant response of the LSC flow occurs when $\delta(t)$ is strongly correlated with $\Omega(t)$ and produces the optimal driving force for oscillations in $\dot\theta(t)$.

In summary, we present the first experimental study of the dynamics of the LSC in turbulent thermal convection in response to modulated rotation. These findings may, to some extent, shed new light on the nature of the large-scale flows in turbulent convection, and be relevant to observed phenomena in astrophysical and geophysical systems.

Acknowledgements

This work was supported by the National Science Foundation of China through grant no. 11202151, the Shanghai Pujiang Program 13PJ1408800 and the Fundamental Research Funds for the Central Universities. S.S. thanks the Twente Mobility Fund for financial support.

References

Ahlers, G., Grossmann, S. & Lohse, D. 2009 Heat transfer and large scale dynamics in turbulent Rayleigh–Bénard convection. *Rev. Mod. Phys.* **81**, 503–537.

Araujo, F. F., Grossmann, S. & Lohse, D. 2005 Wind reversals in turbulent Rayleigh–Bénard convection. *Phys. Rev. Lett.* **95**, 084502.

Assaf, M., Angheluta, L. & Goldenfeld, N. 2012 Effect of weak rotation on large-scale circulation cessations in turbulent convection. *Phys. Rev. Lett.* **109**, 074502.

Avila, M., Belisle, M. J., Lopez, J. M., Marques, F. & Saric, W. S. 2008 Mode competition in modulated Taylor–Couette flow. *J. Fluid Mech.* **601**, 381–406.

Brown, E. & Ahlers, G. 2006 Effect of the Earth's coriolis force on the large-scale circulation of turbulent Rayleigh–Bénard convection. *Phys. Fluids* **18**, 125108.

BROWN, E. & AHLERS, G. 2007 Large-scale circulation model for turbulent Rayleigh–Bénard convection. *Phys. Rev. Lett.* **98**, 134501.

BROWN, E. & AHLERS, G. 2008 A model of diffusion in a potential well for the dynamics of the large-scale circulation in turbulent Rayleigh–Bénard convection. *Phys. Fluids* **20**, 075101.

BROWN, E., NIKOLAENKO, A. & AHLERS, G. 2005 Reorientation of the large-scale circulation in turbulent Rayleigh–Bénard convection. *Phys. Rev. Lett.* **95**, 084503.

BUSSE, F. H. 2000 Homogeneous dynamos in planetary cores and in the laboratory. *Annu. Rev. Fluid Mech.* **32**, 383–408.

CHILLÁ, A. F. & SCHUMACHER, J. 2012 New perspectives in turbulent Rayleigh–Bénard convection. *Eur. Phys. J.* E **35**, 1–25.

DOAKE, C. S. M. 1977 Possible effect of ice ages on Earth's magnetic field. *Nature* **267**, 415–417.

DONNELLY, R. J. 1964 Experiments on the stability of viscous flow between rotating cylinders. III. Enhancement of stability by modulation. *Proc. R. Soc. Lond.* A **281**, 130–139.

FUNFSCHILLING, D. & AHLERS, G. 2004 Plume motion and large-scale circulation in a cylindrical Rayleigh–Bénard cell. *Phys. Rev. Lett.* **92**, 194502.

GEURTS, B. J. & KUNNEN, R. P. J. 2014 Intensified heat transfer in modulated rotating Rayleigh–Bénard convection. *Intl J. Heat Fluid Flow* **49**, 62–68.

HALL, P. 1975 The stability of unsteady cylinder flows. *J. Fluid Mech.* **67**, 29–63.

HART, J. E., KITTELMAN, S. & OHLSEN, D. R. 2002 Mean flow precession and temperature probability density functions in turbulent rotating convection. *Phys. Fluids* **14**, 955–962.

KONING, A. & DUMBERRY, M. 2013 Internal forcing of Mercury's long period free librations. *Icarus* **223**, 40–47.

KRISHNAMURTI, R. & HOWARD, L. N. 1981 Large scale flow generation in turbulent convection. *Proc. Natl Acad. Sci. USA* **78**, 1981–1985.

KUNNEN, R. P. J., CLERCX, H. J. H. & GEURTS, B. J. 2008 Breakdown of large-scale circulation in turbulent rotating convection. *Eur. Phys. Lett.* **84**, 24001.

KUNNEN, R. P. J., STEVENS, R. J. A. M., OVERKAMP, J., SUN, C., VAN HEIJST, G. F. & CLERCX, H. J. H. 2011 The role of Stewartson and Ekman layers in turbulent rotating Rayleigh–Bénard convection. *J. Fluid Mech.* **688**, 422–442.

LOHSE, D. & XIA, K.-Q. 2010 Small-scale properties of turbulent Rayleigh–Bénard convection. *Annu. Rev. Fluid Mech.* **42**, 335–364.

MARSHALL, J. & SCHOTT, F. 1999 Open-ocean convection: observations, theory and models. *Rev. Geophys.* **37**, 1–64.

MIESCH, M. S. 2000 The coupling of solar convection and rotation. *Solar Phys.* **192**, 59–89.

MIYAGOSHI, T. & HAMANO, Y. 2013 Magnetic field variation caused by rotational speed change in a magnetohydrodynamic dynamo. *Phys. Rev. Lett.* **111**, 124501.

NIEMELA, J. J., BABUIN, S. & SREENIVASAN, K. R. 2001 The wind in confined thermal convection. *J. Fluid Mech.* **449**, 169–178.

NIEMELA, J. J., BABUIN, S. & SREENIVASAN, K. R. 2010 Turbulent rotating convection at high Rayleigh and Taylor numbers. *J. Fluid Mech.* **649**, 509–522.

NIEMELA, J. J., SMITH, M. R. & DONNELLY, R. J. 1991 Convective instability with time-varying rotation. *Phys. Rev.* A **44**, 8406–8409.

OLSON, P. 2013 Experimental dynamos and the dynamics of planetary cores. *Annu. Rev. Earth Planet. Sci.* **41**, 153–181.

RESAGK, C., DU PUITS, R., THESS, A., DOLZHANSKY, F. V., GROSSMANN, S., ARAUJO, F. F. & LOHSE, D. 2006 Oscillations of the large scale wind in turbulent thermal convection. *Phys. Fluids* **18**, 095105.

SONG, H., BROWN, E., HAWKINS, R. & TONG, P. 2014 Dynamics of large-scale circulation of turbulent thermal convection in a horizontal cylinder. *J. Fluid Mech.* **740**, 136–167.

SREENIVASAN, K. R., BERSHADSKII, A. & NIEMELA, J. J. 2002 Mean wind and its reversal in thermal convection. *Phys. Rev.* E **65**, 056306.

THOMPSON, K. L., BAJAJ, K. M. S. & AHLERS, G. 2002 Traveling concentric-roll patterns in Rayleigh–Bénard convection with modulated rotation. *Phys. Rev.* E **65**, 046218.

XI, H.-D., ZHOU, S.-Q., ZHOU, Q., CHAN, T.-S. & XIA, K.-Q. 2009 Origin of the temperature oscillation in turbulent thermal convection. *Phys. Rev. Lett.* **102**, 044503.

ZHONG, J.-Q. & AHLERS, G. 2010 Heat transport and the large-scale circulation in rotating turbulent Rayleigh–Bénard convection. *J. Fluid Mech.* **665**, 300–333.

ZHONG, J.-Q., STEVENS, R. J. A. M., CLERCX, H. J. H., VERZICCO, R., LOHSE, D. & AHLERS, G. 2009 Prandtl-, Rayleigh-, and Rossby-number dependence of heat transport in turbulent rotating Rayleigh–Bénard convection. *Phys. Rev. Lett.* **102**, 044502.